Int. J. Multiphase Flow Vol. 9, No. 3, pp. 259–267, 1983
Printed in Great Britain.

0301-9322/83/030259-09$03.00/0
Pergamon/Elsevier

GAS JETS IN FLUIDIZED BEDS: THE INFLUENCE OF PARTICLE SIZE, SHAPE AND DENSITY ON GAS AND SOLIDS ENTRAINMENT

M. FILLA, L. MASSIMILLA and S. VACCARO
Istituto di Chimica Industriale e Impianti Chimici, Università di Napoli,
Istituto di Ricerche sulla Combustione, C.N.R.
Piazzale V. Tecchio, 80125 Napoli, Italy

(*Received* 26 *July* 1982; *in revised form* 5 *December* 1982)

Abstract—Gas has been injected in two-dimensional fluidized beds of solids different in size, density and shape. The ranges of solids sizes and bed heights were such as to produce relatively steady permanent jets.

The mechanics of dispersion of these jets has been studied measuring jet angles, jet gas and solids velocity profiles, and particle entrainment velocities. The proportions of total mass and momentum flowrates pertaining to gas and solids have been calculated from these data.

1. INTRODUCTION

The dispersion of gas in fluidized beds has a considerable influence on the performance of a number of operations such as catalytic reactions (Behie & Kehoe 1973), fluid-bed gas cleaning (Doganoglu *et al.* 1978), ore calcination (Goldney & Hoare 1968).

Injecting gas vertically upwards in a fluidized bed results in the formation of a bubble plume or a permanent jet, depending on bed particle size (Donsì *et al.* 1980b; Yang & Keairns 1980). Jet formation prevails with solids of sizes of the order of 1 mm. In deep beds, bubbles form periodically at the tip of the jet, this retracting back to the orifice after each bubble detachment and moving forth again at the beginning of the next cycle. In shallow beds steady jets are obtained which emerge at the top of the bed, like spouts in spouted beds. Under the experimental conditions of this work acceptable jet steadiness has been found when the bed height was the minimum at which jet necking and bubble formation could be observed.

A distinctive feature of gas jets in fluidized beds is the simultaneous entrainment of bed gas and solids into the jet. Since the pioneering work of Shakhova (1968), other Authors (Donadono *et al.* 1980; Yang & Keairns 1980; Filla *et al.* 1981) have found experimentally that at least to a first approximation there is similarity between transverse gas and solids velocity profiles in jets in fluidized beds, and that these profiles are of the Schlichting or Tollmien type as for homogeneous jets (Abramovich 1963). Accordingly, turbulent jet theory has been used to interpret the behaviour of gas dispersions in fluidized beds (Merry 1971; Shakhova & Minaev 1972; Shakhova & Lastovceva 1973; De Michele *et al.* 1977; Donadono *et al.* 1980; Donsì *et al.* 1980a; Yang & Keairns 1980; Filla *et al.* 1981).

The purpose of this work is that of studying the influence of particle size, density and shape on the mechanics of jets in fluidized beds. A systematic investigation has been carried out to this end using pairs of solids whose physical properties are reported in table 1. Each pair has been tested to investigate the effect exerted on jet dispersion by changing one solids property in turn, namely: the pair acrylic spheres–glass spheres, as regards the effect of density, the pair glass ballotini–glass spheres, as regards that of size, the pairs acrylic spheres–polycarbonate cylinders and glass ballotini–limestone as regards that of shape. Preliminary results with the last pair of materials were presented in a previous paper (Filla *et al.* 1981). The experimental results have been worked out to calculate gas and solids mass and momentum flowrates, and voidage at different heights in the jet.

Table 1. Solids properties and operating conditions

Solids tested	Symbols	Actual fluidization velocity U_f (cm/s)	Ratio to minimum fluidizing velocity U_f/U_{mf}	Particle density ρ_s (g/cm^3)	Particle diameter d_p (mm)	Bed height H_b (cm)	Particles average axis ratio
Glass ballotini	○	78	1.5	2.5	0.7–1.0	8.0	1.0
Limestone	●	78	1.6	2.5	0.7–1.0	8.0	1.6
Acrylic spheres	△	125	1.3	1.2	2.8–3.0	11.0	1.0
Polycarbonate cylinders	▲	125	1.3	1.2	2.8–3.0	11.0	1.0–1.2
Glass spheres	□	260	1.6	3.0	2.8–3.0	10.0	1.0

2. APPARATUS AND EXPERIMENTAL TECHNIQUE

The 390 × 16 mm × mm rectangular cross section column shown in figure 1 has been used. The bed of particles was fluidized by air through a brass perforated plate distributor. The air jet was discharged through a 6 × 16 mm × mm nozzle on the vertical symmetry plane of the column, flush to the distributor. A 4 mm thick perforated plate was inserted on the air supply line to the jet nozzle in order to minimize disturbances of the gas flowrate due to fluctuations of pressure in the bed. A sketch of the jet with the indication of the variables characterizing the geometry is presented in figure 2. Solids properties are given in table 1, together with bed operating conditions. The actual fluidizing velocities were slightly above the minimum in order to prevent defluidization in the neighbourhood of the orifice. The inlet gas velocity at the orifice was 60 m/s in all experiments.

Pitot tube measurements were used to determine jet gas axial and transverse velocity profiles by a 0.7 mm O.D. Pitot probe whose tap hole was partially filled by a protruding steel wire in order to prevent errors due to the momentum of attrited particles in conjunction with the limestone experiments. High speed (1000–5000 f.p.s.) ciné-films of the transparent column wall read at a N.A.C. analyzer provided jet half angles, velocities of particles entering laterally into the jet, and jet particle axial velocities. The procedure described by Donadono & Massimilla (1978) was adopted to evaluate jet half angles θ from motion pictures as shown in figure 3. Alternatively, jet boundaries and values of θ were obtained from Pitot tube measurements by spotting bed loci where the jet gas velocity decayed to the value of the bed fluidizing velocity. It was

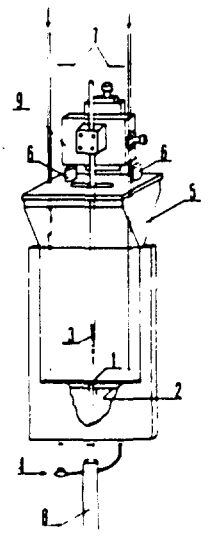

Figure 1.

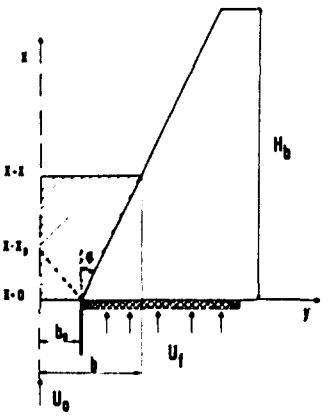

Figure 2.

Figure 1. Apparatus: (1) gas nozzle; (2) perforated plate; (3) pitot tube; (4) fluidizing air line; (5) disengagement section; (6) gas exit; (7) recycle line; (8) jet air line; (9) micrometrical x–y slide.

Figure 2. Jet and bed configuration, and control volume for momentum balance.

assumed that wall effects on measured particle velocities were negligible on the basis of the conclusion drawn by Lefroy & Davidson (1969) for half circular and circular spouted beds of solids of the same sizes as those tested in this work.

3. EXPERIMENTAL RESULTS

Dimensionless gas velocities at the jet centreline (U_m/U_0 where U_m is the velocity at the centreline, U_0 is the velocity at the outlet nozzle) are reported as a function of the dimensionless distance from the nozzle (x/b_0 where x is the distance from the outlet and b_0 is half the width of the outlet nozzle) in figure 4. This figure shows that gas velocity decay is more rapid: for spherical with respect to non-spherical particles of the same density and size; for heavier with respect to lighter particles of the same shape and size; for coarser with respect to finer particles of the same shape and density.

In agreement with previous results (Donsì *et al.* 1980a), figure 4 further shows that a significant potential core penetration is found only with the finer materials tested.

The gas transverse velocity U profiles in the dimensionless form $(U - U_f)/(U_m - U_f)$, where U_m is the velocity on the centreline and U_f the actual fluidization velocity, in function of the dimensionless jet width ($\xi = y/b$) are similar for equal dimensionless distances from the nozzle. The similarity of these profiles, which closely recall those reported previously by Donadono *et al.* (1980) and Filla *et al.* (1981), has been tested by comparing the integrals of the experimental velocity transverse distribution $A = \int_0^1 f_U(\xi)\,d\xi$ and $B = \int_0^1 f_U^2(\xi)\,d\xi$ (used in section 4) with those given by the Schlichting profiles for the initial and main jet region of homogeneous jets. In general, there is a fair agreement between the various values of A and B, as shown in table 2. It appears, in particular, that the values of A and B from experimental profiles at both $x/b_0 = 3$ and $x/b_0 = 6$ are closer to those given by the Schlichting profile for the initial jet region. This is so even though at $x/b_0 = 6$ the transverse profiles should be those typical of the main jet region, particularly for the coarser solids. Figure 4 indicates in fact that the jet potential core penetration x_p is much smaller than $6b_0$ in beds of such materials. The data of table 2 further suggest that the values of A and B are influenced by changes in the size of the particles more than by changes in their shape and density.

The jet half angle is slightly larger for spherical than for non-spherical particles of the same density and size, and tends to increase with increasing size and density of solids, as shown in table 2. Two sets of values of the jet half angle θ_p and θ_t are given. The measurements by

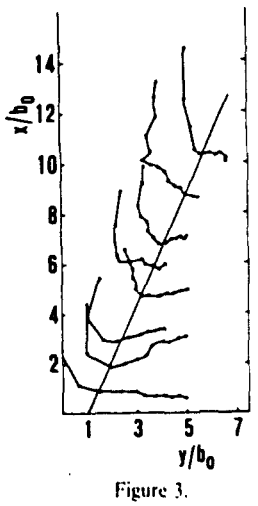

Figure 3.

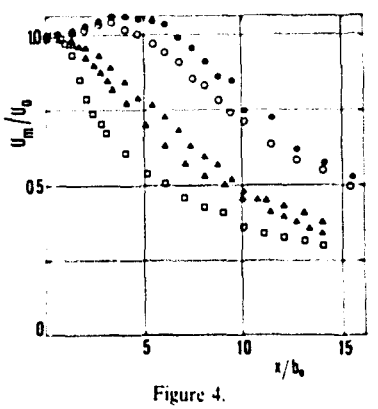

Figure 4.

Figure 3. Particle trajectories and jet expansion angle for glass spheres (2.8–3.0 mm). Distances between two dots covered in about 5.0×10^{-1} s.

Figure 4. Ratio of gas velocity on the jet centreline to that at the nozzle versus distance in orifice half-widths (key to symbols in table 1).

Table 2. Similarity tests of gas velocity distribution, and jet expansion angles

	Glass ballotini 0.7–1.0 mm		Limestone 0.7–1.0 mm		Acrylic spheres 2.8–3.0 mm		Polycarbonate cylinders 2.8–3.0 mm		Glass spheres 2.8–3.0 mm		Schlichting profiles initial region†	Schlichting profiles main region‡
	$x/b_0 = 3$	$x/b_0 = 6$	$x/b_0 = 3$	$x/b_0 = 6$	$x/b_0 = 3$	$x/b_0 = 6$	$x/b_0 = 3$	$x/b_0 = 6$	$x/b_0 = 3$	$x/b_0 = 6$		
$= \int_0^1 f_U(\xi)\,d\xi$	0.54	0.56	0.54	0.55	0.57	0.61	0.58	0.56	0.64	0.61	0.55	0.45
$= \int_0^1 f_U^2(\xi)\,d\xi$	0.40	0.41	0.41	0.41	0.42	0.45	0.41	0.40	0.50	0.46	0.42	0.32
θ_p	20°	13°	19°	12°	33°	21°	27°	21°	32°	26°		
θ_t	$0 \le x/b_0 \le 6$ 17°		$0 \le x/b_0 \le 6$ 17°		$0 \le x/b_0 \le 14$ 22°		$0 \le x/b_0 \le 14$ 21°		$0 \le x/b_0 \le 11$ 24°			

†$f_U = (U - U_f)/(U_m - U_f) = 1 - (1 - (1 - \xi)^{1.5})^2$.
‡$f_U = (U - U_f)/(U_m - U_f) = (1 - \xi^{1.5})^2$.

:ans of the Pitot tube technique gave two different values θ_p at the heights $x/b_0 = 3$ and $b_0 = 6$ showing that the rate of expansion decreases with the distance from the nozzle. The lues θ_t derived from the particle trajectories are obtained over the range of distances from : orifice also indicated in table 2 for each material. As shown in figure 3 this technique tually gives the slope θ_t of the line representing the jet boundary as an average.

Confirming previous findings of Donadono & Massimilla (1978) for comparable experimental nditions as regards bed width to orifice size and to bed height ratios, particles entered into the approximately perpendicular to the jet axis. Their velocity V_y first decreased with distance ım the nozzle to increase slightly again as the bed level where jet necking occurred was proached. This is shown in figure 5, where V_y is reported for the various materials in the rm of regression curves collecting experimental data. For the pair glass ballotini–limestone : experimental points are also reported. For this pair V_y is larger for spherical than for non herical particles, particularly in the neighbourhood of the nozzle. Differences in the pair rylic spheres–polycarbonate cylinders are in the same direction but less pronounced. V_y is ınd to be larger for lighter than for heavier particles of the same size and shape. Increasing rticle size definitely increases the solids entrainment velocity throughout the jet height. Solids trainment velocities fitted by least squares 3rd degree polynomials give by integration the

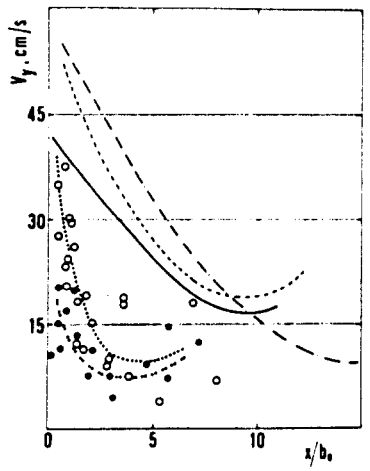

Figure 5. Lateral velocities of solids entrained into the jet vs dimensionless distance from the orifice: · · · · · ·, glass ballotini; · · · · · ·, limestone; — · — · — · —, acrylic spheres; ------, polycarbonate cylinders; ————, glass spheres.

solids mass flowrates entrained into the jet W_{sl} such as

$$W_{sl}(x) = \int_0^x \rho_s V_y (1 - \epsilon_b) t \, dx \qquad [1]$$

where ρ_s is the solids density, V_y the solids velocity at the point of entry into the jet, ϵ_b the bed voidage and t is the two-dimensional jet thickness. These are reported in figure 6 for each material in dimensionless form with respect to the orifice gas mass flowrate.

Particle velocities on the jet centreline V_m reported in figure 7 tend to be lower for spherical than for non-spherical particles of the same size and density. This behaviour is more pronounced for the pair acrylic spheres–polycarbonate cylinders than for glass ballotini–limestone. For given size and shape, coarser and heavier particles are slower, and reach asymptotic velocities more rapidly.

4. CALCULATION OF THE GAS AND SOLIDS MASS AND MOMENTUM FLOWRATES

For a two-dimensional jet of thickness t the solids and gas mass and momentum flowrates in terms of the axial profiles of the jet half-width $b(x)$, gas and solids velocity and voidage on the jet axis $U_m(x)$, $V_m(x)$, $\epsilon_m(x)$, and of the transverse distributions of gas velocity $f_U(\xi)$, solids velocity $f_V(\xi)$ and voidage $f_\epsilon(\xi)$, are:

$$W_s(x) = t\, b(x) \rho_s V_m(x) \left[\int_0^1 f_V \, d\xi - \epsilon_m(x) \int_0^1 f_V f_\epsilon \, d\xi \right] \qquad [2]$$

$$W_g(x) = t\, b(x) \rho_g U_m(x) \epsilon_m(x) \int_0^1 f_U f_\epsilon \, d\xi \qquad [3]$$

$$M_s(x) = t\, b(x) \rho_s V_m^2(x) \left[\int_0^1 f_V^2 \, d\xi - \epsilon_m(x) \int_0^1 f_V^2 f_\epsilon \, d\xi \right] \qquad [4]$$

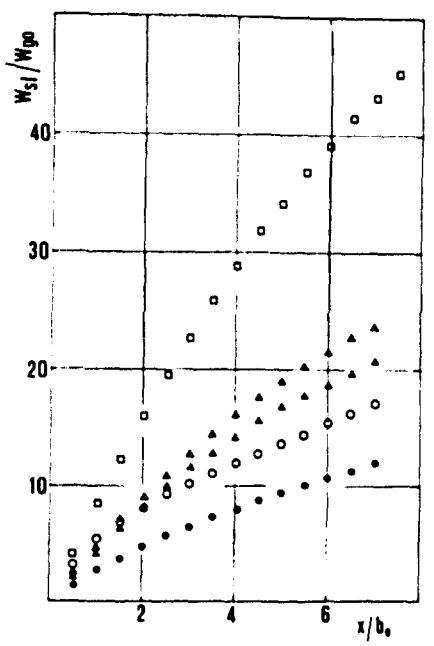

Figure 6. Ratio of solids mass flowrate entrained into the jet to the gas mass flowrate at the nozzle vs distance in orifice half-widths.

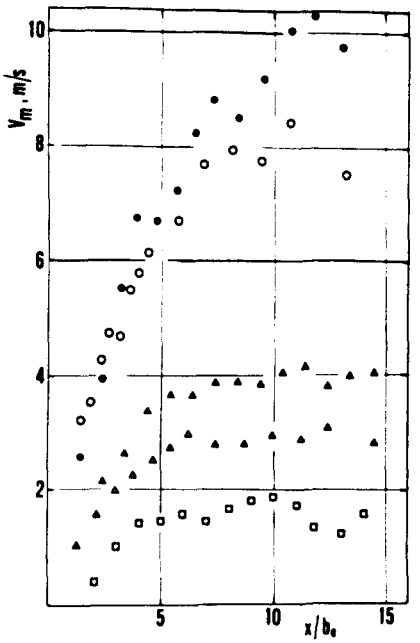

Figure 7. Axial velocities of particles on the jet centreline vs distance from the nozzle in orifice half-widths.

$$M_g(x) = t\, b(x)\rho_g U_m^2(x)\epsilon_m(x) \int_0^1 f_U^2 f_\epsilon \, d\xi. \qquad [5]$$

The total momentum flowrate must satisfy the macroscopic momentum balance on the control volume between $x = 0$ and $x = x$ in figure 2, so that:

$$M_s(x) + M_g(x) = M_0 + F_{J,B}(x) - F_{J,G}(x) \qquad [6]$$

where M_0 is the momentum flowrate of gas at the nozzle, $F_{J,B}$ the buoyancy due to the difference in the densities of the fluidized bed and the jet, and $F_{J,G}$ the gravity force due to the weight of particles contained in the jet control volume. Equation [6] implicitly assumes that momentum exchange between gas and solids and collision between solids is perfect, i.e. without losses.

Equations [2]–[6] form a closed system of equations for the unknowns $W_s(x)$, $W_g(x)$, $M_s(x)$, $M_g(x)$ and $\epsilon_m(x)$. The system has been solved using the axial velocity profiles $U_m(x)$ and $V_m(x)$ for gas and solids, and the transverse profiles $f_U(\xi)$ of gas velocities obtained from experiments. The jet width was that determined by means of the Pitot tube technique described in section 2. The transverse profiles $f_V(\xi)$ of solids velocities were those derived from Schlichting's equation as suggested by Donadono *et al.* (1980). Following these authors, the voidage profile was assumed in the form:

$$f_\epsilon(\xi) = 1 \qquad \text{for} \qquad 0 \le \xi \le \xi^*$$
$$f_\epsilon(\xi) = \epsilon_b/\epsilon_m \qquad \text{for} \qquad \xi^* \le \xi \le 1$$

with $\xi^* = 0.70$ and $\epsilon_b = 0.50$ for all materials tested. This voidage profile accounts for the Shakova (1968) outer jet portion which has the same voidage ϵ_b as the fluidized bed.

The calculated momentum and mass flowrates are presented in table 3 in form of percentages of the total momentum and mass flowrates pertaining to the gas and solids components of the jet admixture at the two dimensionless distances from the nozzle tested. The jet voidage ϵ_m at a given distance from the orifice, and the gas mass flow rate (W_{gl}/W_{g0}) entrained up to that distance made dimensionless with respect to that at the orifice are also given in table 3.

Table 3. Jet gas and solids mass and momentum flowrates, and voidage

	Glass spheres 2.8–3.0 mm		Acrylic spheres 2.8–3.0 mm		Polycarbonate cylinders 2.8–3.0 mm		Glass ballotini 0.7–1.0 mm		Limestone 0.7–1.0 mm	
	$x/b_0 = 3$	$x/b_0 = 6$	$x/b_0 = 3$	$x/b_0 = 6$	$x/b_0 = 3$	$x/b_0 = 6$	$x/b_0 = 3$	$x/b_0 = 6$	$x/b_0 = 3$	$x/b_0 = 6$
$(M_s/(M_s + M_g)) \cdot 100$	56.0	66.3	29.3	51.6	26.3	47.9	16.9	23.6	11.0	13.5
$(M_g/(M_s + M_g)) \cdot 100$	44.0	33.7	70.7	48.4	73.7	52.1	83.1	76.4	89.0	86.5
$(W_s/(W_s + W_g)) \cdot 100$	96.8	97.6	92.0	94.4	90.0	93.1	88.8	92.8	82.4	89.1
$(W_g/(W_s + W_g)) \cdot 100$	3.2	2.4	8.0	5.6	10.0	6.9	11.2	7.2	17.6	10.9
ϵ_m	0.69	0.76	0.81	0.82	0.86	0.90	0.99	0.99	0.99	0.99
W_s/W_{s0}	24.8	33.2	12.5	17.2	9.9	14.2	8.9	15.2	5.3	10.0
W_{gl}/W_{g0}	− 0.18	− 0.20	0.09	0.02	0.10	0.05	0.12	0.18	0.13	0.23
$((W_s - W_{sl})/W_{sl}) \cdot 100$	9.7	−14.8	− 0.7	−19.1	− 3.6	−23.7	−13.1	− 1.8	−18.6	− 6.5

It may be worth noting that values of $W_{sl}(x)$ calculated from [1] on the basis of the experimental values of V_y should equal those of $W_s(x)$ from [2], as the mass flowrate of solids entrained up to the distance x from the orifice should coincide with that transported through the cross section of the jet at that distance. The agreement between $W_{sl}(x)$ and $W_s(x)$ is a measure of the consistency of the experimental data and of the calculation procedure.

5. DISCUSSION

Gas and solids momentum flowrates. A common qualitative feature of the results in table 3 is the increase of the momentum flowrate of solids with increasing distance from the orifice. Quantitatively, the results show that the solids momentum flowrate can reach and overtake that of the gas for the larger size particles in the range of distances investigated. The momentum flowrate apportioned to the solids $M_s/(M_s + M_g)$ decreases in the order: glass spheres, acrylic spheres, polycarbonate cylinders, glass ballotini, limestone. This suggests that the rate of momentum exchange between gas and solids increases with particle size for the same density and shape, with particle density for the same shape and size, with particle sphericity for the same size and density. These trends agree with those shown by the jet angle (table 2), and by the axial decay of the gas velocity on the jet centreline (figure 4).

It is well known for homogeneous jets that increasing the density of the dispersing medium enhances the rate of momentum transfer from the injected gas. Apparently, this behaviour holds also in the case of heterogeneous jets, from a comparison of the rates of momentum transfer between gas and particulate phase of fluidized solids of different densities.

In the view that the jet boundary is defined by a dynamic equilibrium between the rate at which the dense phase supplies particles to the jet and that at which they are swept away by the jet gas, it may be inferred that the resistance of the particulate phase to the transverse flow towards the dilute region of the jet is larger the smaller and the lighter the particles, and also larger for non-spherical than for spherical particles.

Gas and solids entrainment rates. Jet solids mass flowrates increase in all cases with distance from the nozzle. The solids fraction mass flowrates $W_s/(W_s + W_g)$ for solids of different shape, size and density decrease in the same order previously outlined concerning the decrease of $M_s/(M_s + M_g)$. This trend is consistent with that shown by the solids entrainment flowrates in figure 6. Note that the jet mass flowrate is concentrated in the solids component for all materials tested, the gas portion $W_g/(W_s + W_g)$ being generally below 10%.

Values of lateral gas flow W_{gl} entrained at a given height can be obtained as the difference between W_g at that height and W_{g0}. Figure 8 gives W_{gl}/W_{g0} as a function of x/b_0 for four materials tested. An interesting general result is that W_{gl}/W_{g0} passes through a maximum within the range of distances from the nozzle investigated. This trend suggests that there is a region of gas entrainment close to the nozzle, followed by gas disentrainment further up. This maximum moves closer to the orifice for coarser, denser and more spherical particles. An extreme case of

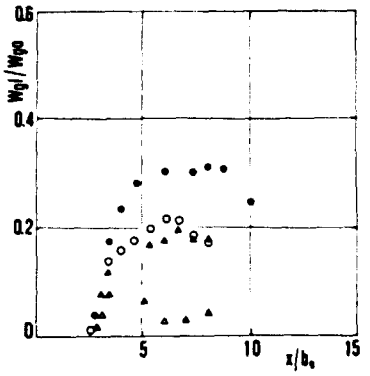

Figure 8. Ratio of gas mass flowrate entrained into the jet to that at the nozzle in function of distance from the nozzle in orifice half-widths.

this behaviour has been found in this work for glass spheres 2.8–3.0 mm, where the gas disentrainment region has already overtaken that of gas entrainment as close to the nozzle as $x/b_0 = 3$. A similar result has been found by Yang & Keairns (1980). Whereas there is little doubt about the trend of W_{gl} with distance from the orifice, the absolute values may be affected by significant errors because W_{gl} is a small difference between large numbers.

Voidage. The voidage on the jet centreline follows the trend of the gas mass flowrate, as may be expected. The upper bound of unity is closely approached within the range of distances investigated by particles below 1 mm. It falls to much lower values with increasing particle size and density.

6. CONCLUSIONS

Permanent, steady jets can be obtained by injecting gas in fluidized beds of tested solids provided bed heights are kept below those of incipient bubble detachment. Jet gas transverse velocity profiles conform to the Schlichting type.

Effects of particle characteristics have been found on the mechanics of jet dispersion, the relevance of shape, density and size increasing in this order for the experimental conditions of this work. The effects investigated include jet angle, axial jet gas and solids velocities, gas velocity transverse profiles and lateral solids entrainment velocities.

Jet voidage, and gas and solids mass and momentum flowrates have been worked out from these data. Voidage decreases with particle size. Jet momentum divides differently between solids and gas phases of the admixture. For finer materials it is mainly apportioned to the gas phase, whereas for coarser materials tends to a more even distribution between the two components. The solids fraction of the mass flowrate is dominant in all cases with a tendency to increase for coarser solids. Evaluation of gas jet flowrate at different heights shows that there is a region of gas entrainment close to the orifice followed by gas disentrainment further up.

REFERENCES

Abramovich, G. N. 1963 *The Theory of Turbulent Jets.* M.I.T. Press, Cambridge, Mass.

Behie, L. A. & Kehoe, P. 1973 The Grid Region in a Fluidized Bed Reactor. *AIChE J.* 19, 1070–1073.

De Michele, G., Donsì, G. & Massimilla, L. 1977 Heat transfer between jet and fluidized beds. *European Congress on: "Transfer Processes in Particle Systems"*, Nuremberg, 28–30 March.

Doganoglu, Y., Jog, V., Thambimuthu, K. V. & Clift, R. 1978 Removal of fine particulates from gases in fluidized beds. *Trans. Inst. Chem. Engrs* 56, 239–248.

Donadono, S. & Massimilla, L. 1978 Mechanism of momentum and heat transfer between gas

jets and fluidized beds. *Fluidization* (Edited by DAVIDSON, J. F. & KEAIRNS, D. L.). Cambridge University Press.

DONADONO, S., MARESCA, A. & MASSIMILLA, L. 1980 Gas injection in shallow beds of fluidized coarse solids. *Ing. Chim. Ital.* **16**, 1–10.

DONSÌ, G., MASSIMILLA, L. & COLANTUONI, L. 1980a The dispersion of axisymmetric gas jets in fluidized beds. *Fluidization* (Edited by GRACE, J. R. & MATSEN, J. M.). Plenum Press, New York.

DONSÌ, G., ISCARO, A., MASSIMILLA, L. & ZUCCHINI, C. 1980b Gas jetting in fluidized beds. *Motion Picture, International Fluidization Conference.* Henniker, New Hampshire, 3–8 August.

FILLA, M., MASSIMILLA, L. & VACCARO, S. 1981 Solids entrainment in jets in fluidized beds: the influence of particle shape. *Journées Européennes sur la Fluidisation*, Toulouse, France, 24–25 September.

GOLDNEY, L. H. & HOARE, J. S. 1968 Design and operation of a submerged combustion fluidized bed process for phosphate calcination. *Mech. and Chem. Engng Trans.*, The Institution of Engineers, Australia, November, pp. 181–186.

LEFROY, G. A. & DAVIDSON, J. F. 1969 The mechanics of spouted beds. *Trans. Inst. Chem. Engrs* **47**, T120–T128.

MERRY, J. M. D. 1971 Penetration of a horizontal gas jet in fluidized beds. *Trans. Inst. Chem. Engrs* **49**, 189–195.

SHAKHOVA, N. A. 1968 Outflow of turbulent jets into a fluidized bed. *Inzh. Fiz. Zh.* **14**, 61–69.

SHAKHOVA, N. A. & MINAEV, G. A. 1972 Aerodynamics of jet discharged into a fluidized bed. *Heat Trans. Sov. Res.* **4**, 133–142.

SHAKHOVA, N. A. & LASTOVCEVA, I. N. 1973 On interphase heat transfer into a fluidized layer. *Inzh. Fiz. Zh.* **25**, 581–588.

YANG, W. C. & KEAIRNS, D. L. 1980 Momentum dissipation of and gas entrainment into a gas–solid two-phase jet in a fluidized bed. *Fluidization* (Edited by GRACE, J. R. & MATSEN, J. M.). Plenum Press, New York.